Check for updates

A Journal of the Gesellschaft Deutscher Chemiker
Angewandte Chemie
GDCh
International Edition
www.angewandte.org

## Accepted Article

**Title:** Cooperative Surface Passivation and Hierarchical Structuring of Zeolite Beta Catalysts

**Authors:** Sungmin Han, Noemi Linares, Tanguy Terlier, Jeffrey B. Hoke, Javier García Martínez, Yuejin Li, and Jeffrey D. Rimer

This manuscript has been accepted after peer review and appears as an Accepted Article online prior to editing, proofing, and formal publication of the final Version of Record (VoR). The VoR will be published online in Early View as soon as possible and may be different to this Accepted Article as a result of editing. Readers should obtain the VoR from the journal website shown below when it is published to ensure accuracy of information. The authors are responsible for the content of this Accepted Article.

**To be cited as:** *Angew. Chem. Int. Ed.* **2022**, e202210434

**Link to VoR:** https://doi.org/10.1002/anie.202210434

WILEY-VCH

10.1002/anie.202210434

WILEY-VCH

RESEARCH ARTICLE

# Cooperative Surface Passivation and Hierarchical Structuring of Zeolite Beta Catalysts

Sungmin Han[a], Noemi Linares[b], Tanguy Terlier[c], Jeffrey B. Hoke[d], Javier García Martínez[b], Yuejin Li[d], and Jeffrey D. Rimer*[a]

[a] Dr. Sungmin Han and Prof. J. D. Rimer
Department of Chemical and Biolmolecular Engineering
University of Houston
Houston, TX 77204, USA
E-mail: jrimer@central.uh.edu

[b] Dr. Noemi Linares and Prof. J. García Martínez
Molecular Nanotechnology Lab, Department of Inorganic Chemistry
University of Alicante
Alicante 03690, Spain

[c] Dr. Tanguy Terlier
Shared Equipment Authority, SIMS laboratory
Rice University
Houston, TX 77005, USA

[d] Dr. Jeffrey B. Hoke and Dr. Yuejin Li
BASF Corporation
Iselin, NJ 08830, USA

Supporting information for this article is given via a link at the end of the document.

**Abstract:** We report a method to prepare core-shell zeolite beta (*BEA) with an aluminous core and an epitaxial Si-rich shell. This method capitalizes on the inherent defects in *BEA crystals to simultaneously passivate acid sites on external surfaces and increase intracrystalline mesoporosity through facile post-hydrothermal synthesis modification in alkaline media. This process creates more hydrophobic materials by reducing silanol defects and enriching the shell in silica via a combination of dealumination and the relocation of silica from the core to the shell during intracrystalline mesopore formation. The catalytic consequences of *BEA core-shells relative to conventional analogues were tested using the biomass conversion of levulinic acid and *n*-butanol to *n*-butyl levulinate as a benchmark reaction. Our findings reveal that siliceous shells and intracrystalline mesopores synergistically enhance the performance of *BEA catalysts.

## Introduction

Beta (*BEA) is a commercial large-pore zeolite composed of 3-dimensional (3D) 12-membered ring channels.[1] The structure of *BEA originates from disordered intergrowth of three different polymorphs: A, B, and less frequently observed C.[1a, 2] Zeolite beta consists of two straight channels along its a- and b-directions (0.66 × 0.67 Å), a sinusoidal channel along the c-direction (0.56 × 0.56 Å), and cavities at the intersections of these channels with ca. 1.2 nm diameter.[1c] These topological features provide *BEA crystals with an open framework; therefore, *BEA has been widely used in various catalytic reactions involving larger molecules as reactants or products in applications that include gas-oil cracking,[3] hydrocarbon cracking,[4] benzene alkylation,[5] toluene acylation,[6] and biomass isomerization and conversion[7].

The most commonly accepted mechanism of *BEA crystallization is a nonclassical pathway involving the aggregation of amorphous precursor nanoparticles, followed by their solid-state reorganization into a crystalline product.[8] Prior studies of *BEA synthesis reported particles composed of small crystallites, which can yield a small amount of intercrystallite mesoporosity.[8a, 8d] More recent classical models of *BEA crystallization also predict the generation of mesopores originating from random nucleation and growth of polymorphs A and B.[9] We posit that both classical and nonclassical mechanisms likely contribute to *BEA crystallization and impact the formation of defects. Indeed, numerous studies report a large amount of silanol defects in disordered *BEA polymorphs.[10] This feature has been utilized in methods that modify *BEA structures via dealumination to increase the density of silanol nests.[11] For instance, dealuminated *BEA has been used as a scaffold for incorporating various metal cations, thus introducing new functionality (e.g. Lewis acidity) to improve the catalytic performance of zeolite beta.[11]

This study focuses on the generation of zeolite catalysts with a siliceous exterior surface, which has proven to be an effective technique to suppress the formation of external coke and enforce shape selectivity.[12] Synthesis of core-shell architectures is an efficient method of surface passivation that bypasses the deleterious effects of alternative methods, such as silane functionalization that was commercialized by Dupont and Mobil in the 1980s.[13] In core-shell zeolite syntheses, epitaxial growth of the shell on a parent core, both possessing the same zeolite topology, preserves crystallographic registry. Prior studies of *BEA core-shell preparation have mostly involved core and shell combinations with distinctly different zeolite structures. Examples include *BEA@zeolite Y[14], *BEA@silicate-1[15], and *BEA@amorphous silica[16]. There is one study by Xiao and coworkers reporting epitaxial core-shell *BEA synthesis without the intent of growing passivated (Si-rich) shells.[17] We recently synthesized core-shell zeolites of MFI (ZSM-5@silicalite-1) and MEL (ZSM-11@silicalite-2) via epitaxial growth of the purely siliceous zeolite on the surface of its aluminosilicate

Accepted Manuscript


This article is protected by copyright. All rights reserved.

isostructure.[18] The siliceous shell did not result in loss of micropore volume, and its passivation of the outer rim was also shown to markedly reduce mass transport limitations, leading to a dramatic enhancement in catalytic performance in the methanol-to-hydrocarbon (MTH) reaction.[18b]

Herein we emulate this core-shell design for zeolite beta as a method to both passivate external surfaces and take advantage of intrinsic defects in *BEA to create mesoporous (hierarchical) materials via secondary hydrothermal treatment. Forming zeolites with hierarchical structure is an effective strategy to enhance molecular transport in catalytic reactions.[19] For the purpose of assessing the impact of these new architectures on catalyst performance, we selected the biomass conversion of levulinic acid (LA) to *n*-butyl levulinate (*n*BuLev) as a benchmark reaction. The U.S Department of Energy has highlighted LA as one of the top 15 platform biomass molecules.[20] It has been demonstrated that LA can be converted to numerous value-added molecules, such as γ-valeroractone, levulinate esters, and 2-methyl tetrahydrofuran.[20] Notably, levulinate esters have been of high interest owing to their potential uses as fuel additives, fragrances, and food additives.[20c, 21] Levulinate esters can also be used as precursors for levulinic ketals, which are building blocks of plasticizers.[22] Relatively few studies have explored the synthesis of *n*BuLev,[23] which is a promising fuel additive.[21-22, 24] Among the catalytic studies of LA esterification to *n*BuLev, it has been observed that *BEA outperforms other zeolites (e.g. MFI, MOR, and FAU).[23a] In this study, we report methods to enhance the catalytic performance of *BEA beyond current state of the art catalysts.

## Results and Discussion

We prepared core-shell zeolite *BEA using protocols similar to those reported for zeolite MFI.[18] Crystals prepared as seeds for secondary growth (*Core* sample) followed a procedure by Ding et al.[25] to generate spheroidal particles with an average diameter of 530 nm and a Si/Al ratio of 22. Field emission scanning electron microscopy (FE-SEM) images reveal a rough particle morphology (Figure 1a), which is consistent with transmission electron microscopy (TEM) images showing that each particle is a single crystal composed of smaller crystallite domains in equal registry (Figure S1a). This observation aligns with the proposed growth mechanism of *BEA[8] involving the aggregation of amorphous precursors (Scheme 1) via crystallization by particle attachment (CPA).[26] This nonclassical pathway leads to mesopores (or defects) at interstitial spaces between aggregates. Anderson and coworkers have also modeled *BEA crystallization by a classical mechanism (i.e. monomer addition) that predicts rough exterior surfaces and a high density of defects, which include voids within their structures caused by random nucleation and growth of polymorphs A and B.[9] It is likely that both of these mechanisms occur during the synthesis of *BEA crystals used as seeds (Figure 1a). For samples examined herein we performed a post-synthesis treatment to ensure that all residual amorphous material after secondary growth of core-shells was fully crystallized. The same procedure was performed for the as-synthesized *Core* sample as a reference using a protocol similar to the preparation of finned zeolites.[27] We first tested the annealing process on the Core, which involves the suspension of zeolite crystals in an alkaline solution (pH 11) containing a small quantity of silica (close to the solubility of zeolite beta) and an organic structure-directing agent (tetraethylammonium, TEA). This solution was hydrothermally treated at 170 °C and autogenous pressure for different times. A 3-day annealing of the Core (sample *CA*) retains its general spheroidal shape (Figure 1b), with the exception of more visible protrusions after hydrothermal treatment. The accentuated external roughness of CA was also observed in TEM images (Figure S1b). This sample has enhanced intracrystalline mesoporosity and will be used as a reference to assess the effect of mesoporosity in core-shell samples.

Core-shell *BEA particles were prepared using seeds (*Core* sample) wherein a siliceous *BEA shell was epitaxially grown on the surface of the aluminosilicate *BEA core under hydrothermal conditions. The Al-free mixture used for shell growth contained supersaturated silica and TEA, similar to our protocols for core-shell MFI and MEL.[18] The resulting crystals (sample *CS*) exhibit larger surface protrusions due to shell growth from silicate species in solution (Figures 1c and S1c). The shell growth was also confirmed by dynamic light scattering (DLS) measurements, showing an increase in the hydrodynamic radius from 266 to 288 nm (Figure 1e). Elemental analysis using time-of-flight secondary ion mass spectrometry (ToF-SIMS) revealed an increased Si/Al ratio (Figure 1f) in the outer rim of CS samples relative to the Core. These measurements were consistent with surface-sensitive X-ray photoelectron spectroscopy (XPS) measurements (Figure 1e), showing a higher Si/Al ratio of the core-shell sample. After annealing for 7 days, the treated core-shell (sample *CSA*) exhibits a higher density of surface protrusions with reduced average size (Figures 1d and S1d). This observation differs from our previous study of ZSM-5@silicalite-1, where annealing leads to a smoothening of rough surfaces.[18] One notable difference between CA and CSA is that shell growth preserves the structural integrity of the interior core, whereas direct annealing of as-synthesized *BEA crystals can cause some particles to be broken, as evidenced by electron microscopy (Figure S2). This particle breakage is not associated with crystallinity, i.e. both samples are fully crystalline by powder X-ray diffraction (Figure S3). We attribute this effect to intra-particle structural rearrangement that leads to the generation of intracrystalline mesopores (vide infra).[28] To minimize particle breakage of the CA sample, we selected a shorter (3-day) annealing step.

The cartoons in Scheme 1 highlight the major features of *BEA crystals observed during each stage of core-shell growth and post-synthesis treatment. The first step involving crystallization of seeds (Core) from amorphous precursor aggregates is based on previous models.[8] Key features of Core particles are rough exterior surfaces (highlighted in the inset) and a small quantity of intracrystallite mesopores (indicated by white vacancies). Growth of the core-shell (CS) leads to a minor increase in particle size without altering other features; however, the annealing stage induces the formation of mesopores within the core by a dissolution and reprecipitation process that concomitantly leads to changes in the shell, such as an increased roughness (highlighted in the inset). These structural and morphological changes are consistent with TEM images of particles at each stage (see Figure 2). The sequence in Scheme 1 is also consistent with changes in compositions and textural properties listed in Table 1. The overall Si/Al ratio of samples



This article is protected by copyright. All rights reserved.

Accepted Manuscript

10.1002/anie.202210434


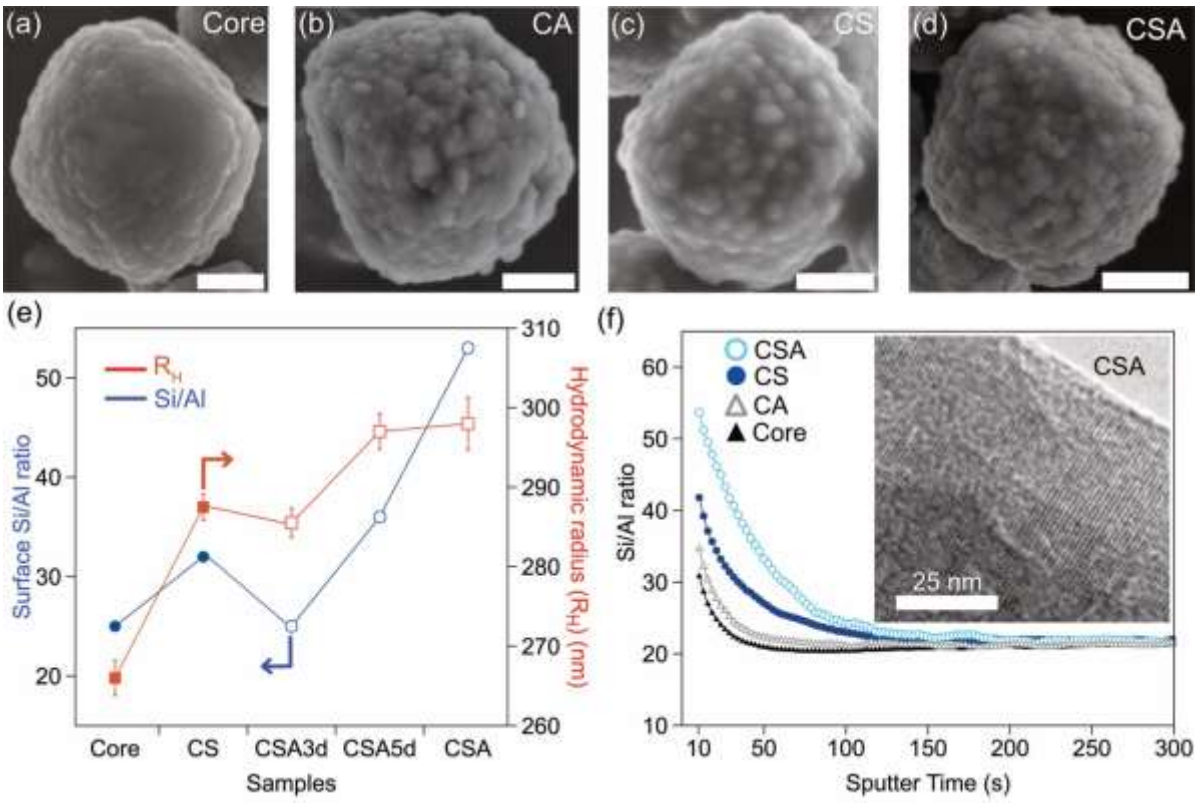


**Figure 1.** Field emission scanning electron micrographs of representative crystals from syntheses of (a) Core, (b) CA, (c) CS, and (d) CSA samples. Scale bars equal 200 nm. (e) Comparison of surface Si/Al ratios measured by XPS (blue, left y-axis) and the hydrodynamic radius (red, right y-axis) measured by DLS for Core and CS samples after various annealing periods (0, 3, 5 days) to form CSA (7 days). Unfilled symbols indicate samples with enhanced mesoporosity. (f) ToF-SIMS measurements of Si/Al ratio as a function of sputtering time for each sample. The inset is a TEM image of CSA showing continuous lattice fringes extending from the interior (core) to the exterior (shell).

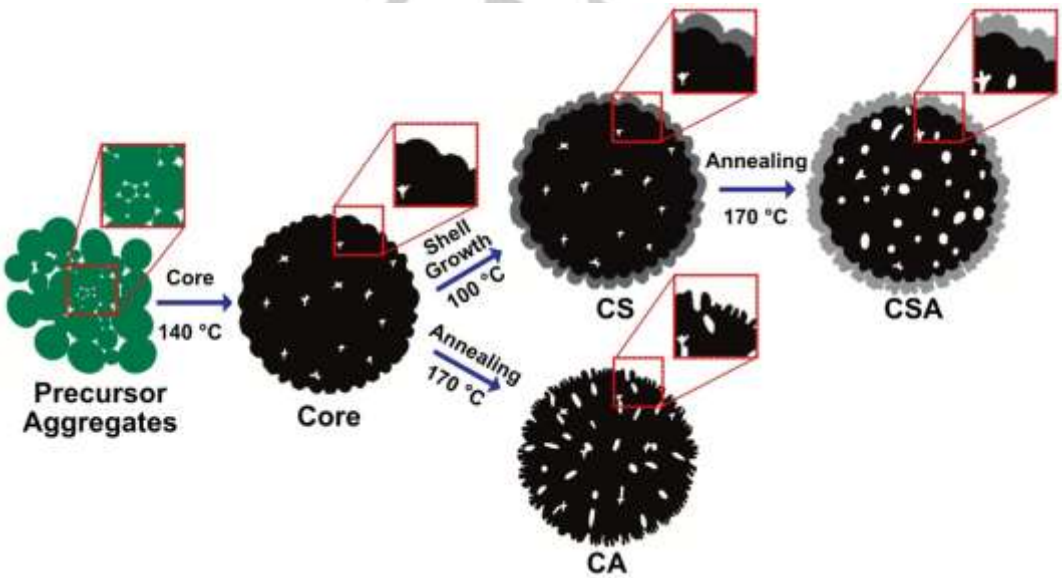


**Scheme 1.** Idealized sequences of *BEA core-shell synthesis under hydrothermal conditions (arrows) beginning from aggregates of amorphous precursors (green) that lead to seed crystals (Core) with intercrystallite mesoporosity, the growth of a siliceous shell (CS) that preserves the mesoporosity, and annealing to generate the final product (CSA) with enhanced intracrystalline mesoporosity and more roughened exterior shells. Direct annealing of the Core (CA) also enhances intracystalline mesoporosity and results in more roughened external surfaces.

measured by energy dispersive X-ray spectroscopy (EDX) exhibit small deviations within the range of 21 – 23. This indicates that shell growth and/or annealing do not appreciably affect the overall composition; however, Si/Al ratios estimated from XPS, which is



Accepted Manuscript

This article is protected by copyright. All rights reserved.

biased to the exterior surface (ca. 7 nm depth), differ in their values depending on post-synthesis surface treatment.(e.g., degree of Si deposition by shell growth). For instance, the original Core sample has a surface Si/Al of 25, which is approximately equal to its overall composition (Si/Al = 22). The 3-day annealed core (CA) has a slightly higher surface Si/Al ratio, suggesting a mild (re)precipitation of silica that is commensurate with the partial dissolution of the core during mesopore generation. The core-shell sample (CS) has an increased surface Si/Al ratio of 32. When considering secondary growth leads to a shell with an average thickness of 20 nm (Figure 1e), which is greater than the depth of XPS measurements, these findings indicate the shell is not completely siliceous owing to a redistribution of aluminum from the core. A similar effect was observed for MFI-type core-shells, although aluminum migration was less severe than that observed in the current study of *BEA (i.e. the external Si/Al ratio was closer to 80 for a MFI shell thickness of ca. 10 nm).[18a] The 7-day annealed *BEA core-shell (CSA) has an increased surface Si/Al ratio of 53, which indicates dealumination of the shell.

The changes in surface Si/Al ratio are evident in ToF-SIMS measurements, which is a sensitive analytical technique that enables the analysis of specific elemental or compound ions as surfaces are etched by heavy cation ($Cs^+$) sputtering. Here, we used $Si^+$ for monitoring silicon signal and $Al^+$ for aluminum. As shown in Figure 1f, the Si/Al ratio of the Core is around 30 at its exterior surface and rapidly decreases with increased sputtering time to a value of 21, which is equivalent to its bulk value measured by EDX (Table 1). This indicates mild Si-zoning in as-synthesized *BEA crystals, which was also observed in MFI-type zeolites.[29] The annealed core (CA) follows the same general trend in Si/Al ratio with sputtering time where the initial Si/Al ratio of 35 is consistent with XPS measurements. ToF-SIMS measurements of core-shell samples CS and CSA reveal exterior Si/Al ratios of 43 and 55, respectively, which also correspond to the trends observed by XPS. All samples exhibit monotonic reductions in Si/Al ratio to values of 21 within the interior, which is expected for core-shell (or zoned) zeolites. These analyses also verify that the relatively siliceous shell of CS is further enriched in silica after annealing (sample CSA). High-resolution TEM images of CSA core-shells (Figure 1e, inset) clearly show lattice fringes that extend from the interior to the exterior, indicating the epitaxial growth of outer layer to generate a shell that is in crystallographic registry with the underlying core.

Here, we systematically examine the impact of annealing duration on core-shell composition and structure. In Figure 1e, we report the changes in surface Si/Al ratio and hydrodynamic radius of core-shell *BEA particles as a function of annealing time. As previously mentioned, the as-synthesize core-shell (CS) has a surface Si/Al ratio of 32 and overall particle radius of 287 nm. Textural analysis of the CS sample reveals a microporosity (Table 1) that is characteristic of *BEA zeolites reported in literature[30] with interparticle mesoporosity (Figure 2a). After 3 days of annealing (sample CSA3d), we observed a decrease in surface Si/Al ratio to 25 and the apparent hysteresis in its $N_2$-isotherm (Figure S4), which is indicated in Figure 1e by unfilled symbols and could be related to formation of larger mesopores. Interestingly, the radius of CSA3d (285 nm) is almost identical to that of CS, suggesting desilication of the shell occurs during the initial period of secondary hydrothermal treatment despite a small concentration of silica in the annealing medium. In previous studies, desilication of zeolites in alkaline media is typically carried out in basic solutions without silica, and leads to the formation of mesopores.[4, 28, 31] When the annealing process is extended to 5 days (sample CSA5d), the Si/Al ratio increases to a value of 36 with a concomitant increase in radius to 296 nm (ca. 9 nm larger than CS). Given that the silica concentration used in the annealing medium is around the solubility of the zeolite, an increased size suggests that nutrient for growth is generated from the interior of the core-shell crystal – meaning that the initial desilication process transitions to one of silica reprecipitation at later times.

Continued annealing for 7 days (sample CSA) results in further increase of the surface Si/Al ratio to 53 without noticeable size increase compared to CSA5d, which still has the overall Si/Al ratio as 23. This seems to indicate dealumination of the shell at later stages of annealing. This is an unexpected observation since dealumination typically occurs in acidic conditions.[11] It has been reported that alkaline leaching of solutions using NaOH and organic structure-directing agents (e.g. tetraalkylammonium ions) leads to slight dealumination along with desilication; however, in these systems the extracted Al species are eventually reintroduced into the zeolite, resulting in an overall reduction in Si/Al ratio.[4, 32] The latter process is believed to be mediated by the presence of the organic structure-directing agent, TEA. In our study, we also used TEA in the annealing solution along with a small quantity of silica and observed a net dealumination. To determine if the presence of silica in solution impacts the annealing process, we conducted a control experiment using an identical annealing solution without a silicon source (Figure S5). Under this condition, CS experienced only desilication to yield a lower surface Si/Al ratio (ca. 22) than that of the original Core (ca. 25). Based on these results, we speculate the presence of silica species in solution facilitates dealumination of the shell during annealing, although the exact mechanism remains elusive.

The conditions selected for secondary growth of shells and annealing affect the acid site density ($C_{acid}$) of *BEA samples. Ammonia temperature-programmed desorption ($NH_3$-TPD) measurements reveal that the more siliceous shell of CS reduces its acid site density by 10% compared to the Core (Table 1). The acid site density of CSA is almost 30% less than the Core owing to additional shell growth and dealumination during the 7-day annealing period. Conversely, the acid site density of CA is nearly 20% more than the Core, which suggests that the combined processes of dealumination and desilication that occur during the 3-day annealing period are dominated by the latter. Additional acid site characterization using pyridine-FT-IR revealed that Core, CS, and CSA samples have an approximate 70:30 split between Brønsted acid sites (BAS) and Lewis acid sites (LAS), whereas CA has slightly higher BAS density (76%). Solid state $^{27}Al$ NMR analysis reveals that the percentage of extra-framework Al (EFAl) falls within a narrow range for all samples (10 – 12%), with the exception of CS that has a slightly higher EFAl content (ca. 19%). Collectively, these results indicate that processes of growth and dissolution during core-shell synthesis and post-synthesis treatments do not appreciably alter aluminum speciation, only the quantity of Al sites (Table 1).



Accepted Manuscript

This article is protected by copyright. All rights reserved.

10.1002/anie.202210434


**Table 1.** Physicochemical properties of as-synthesized and annealed *BEA samples.

| Sample | Si/Al Surface[a] | Si/Al Bulk[b] | $V_{micro}$[c] ($cm^3/g$) | $V_{meso}$[c] ($cm^3/g$) | $V_{tot}$[c] ($cm^3/g$) | $C_{acid}$[d] (μmol/g) | Acid site type[e] (%) | |
|---|---|---|---|---|---|---|---|---|
| | | | | | | | Brønsted | Lewis |
| Core | 25 | 22 | 0.27 | 0.06 | 0.33 | 543 | 70 | 30 |
| CA | 28 | 21 | 0.26 | 0.10 | 0.36 | 642 | 76 | 24 |
| CS | 32 | 22 | 0.27 | 0.04 | 0.31 | 485 | 68 | 32 |
| CSA | 53 | 23 | 0.21 | 0.06 | 0.27 | 381 | 72 | 28 |

[a] Si/Al ratio from XPS; [b] Si/Al ratio from EDX; [c] Estimated by DFT calculations based on experimental $N_2$ adsorption/desorption isotherms (Figure 2a). Total pore volumes ($V_{tot}$) are calculated when $P/P_0$ = 0.95.; [d] $NH_3$-TPD; [e] Measured by pyridine FTIR.

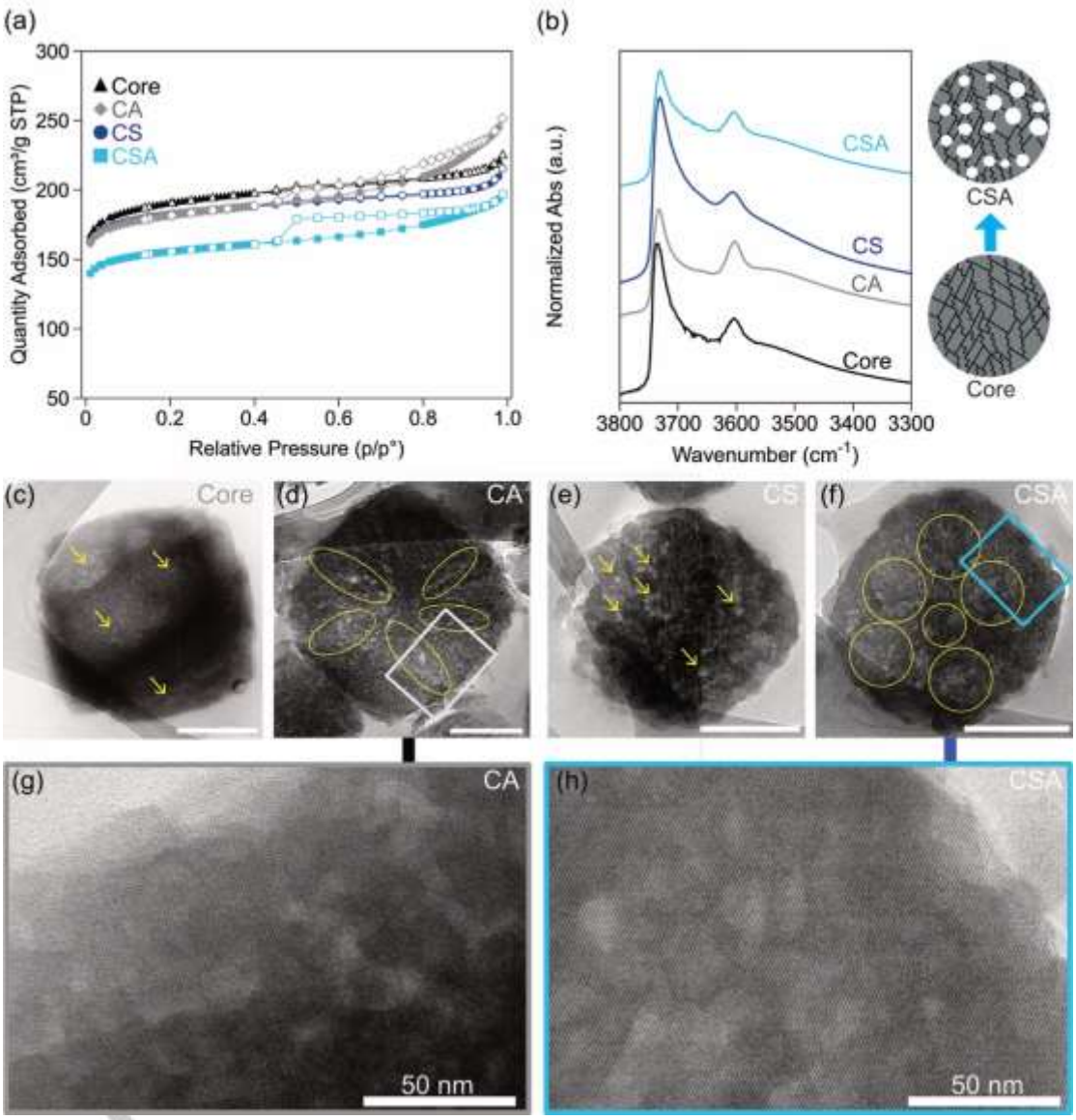


**Figure 2.** (a) $N_2$ adsorption/desorption isotherms and (b) normalized FT-IR spectra (-OH vibration regions) of samples Core, CA, CS, and CSA with a schematic illustrating mesopore formation along boundaries between randomly oriented polymorphs. The area of the Si-(OH)-Al (BAS) vibrational signal at 3610 $cm^{-1}$ was scaled by the concentration of BAS calculated by multiplying $C_{acid}$ by the BAS percentage (Table 1). Inset: idealized depiction of the Core sample with stacking faults (black lines) and the CSA sample with intracrystalline mesopores (white regions). (c – h) Ultramicrotomed cross-section TEM images of (c) Core, (d) CA, (e) CS, and (f) CSA samples. Scale bars equal 200 nm. Areas suspected to be mesopores are highlighted with arrows or elliptical circles. (g and h) Magnified TEM images of boxed regions in panels (d) and (f) for samples CA and CSA, respectively.



Accepted Manuscript

This article is protected by copyright. All rights reserved.

10.1002/anie.202210434


The two annealed samples, CA and CSA, display relatively large hysteresis in their $N_2$ adsorption isotherms (Figure 2a), indicative of intracrystalline mesoporosity that was confirmed by TEM (Figure 2d and f). In contrast, relatively negligible hysteresis is observed from the non-annealed samples Core and CS, which is attributed to the presence of small mesopores (< 4 nm, Figure S7). Interestingly, core-shell synthesis of other zeolites that grow by nonclassical CPA and commonly exhibit defects (e.g. MFI) does not commonly result in hierarchical structure formation.[18] The unique effect observed for *BEA may be attributed in part to its higher propensity for desilication during alkali solution treatment compared to other zeolite structures.[4, 31g] In general, mesopore formation in alkaline media typically begins at crystallite boundaries or defects within zeolite crystals.[31b-d, 31f, 31g] Following this assertion, we analyzed how the annealing process affects silanol defects in Core and CS samples employing FT-IR. For this analysis, we normalized the measured FT-IR spectra based on the total concentration of Brønsted acid sites. FT-IR spectra in Figure 2b show that the majority of silanol groups in all samples are isolated species (3740 $cm^{-1}$) with only a minute quantity of silanol nests (3550 $cm^{-1}$). Samples CA and CSA have lower silanol signals compared to their non-annealed counterparts (Core and CS). This indicates that the annealing process decreases the amount of silanol groups in *BEA during desilication processes that enhance intracrystalline mesoporosity and ultimately leads to a less hydrophilic material.[33]

A reduction in silanol density during mesopore formation is counter to most trends reported in literature for other zeolites.[31b, 31d, 31f, 34] For example, desilication of zeolite ZSM-5 (MFI) in alkaline media leads to increased silanol species that presumably terminate the newly formed mesopores.[31d] Similar effects have been reported for hierarchical USY (FAU) using surfactant treatments.[31b] Here we hypothesize that the unique trend observed for *BEA is attributed in part to the stacking faults that originate from different polymorphs.[10] These stacking faults are putative sites for initiating desilication, as illustrated in Figure 2b, such that mesopore formation has the ability to eliminate silanol groups along polymorph boundaries during annealing by a mechanism that is elusive.

Direct confirmation of mesoporosity was obtained from high-resolution TEM using cross-sectional images of each sample (Figure 2c – h). The relatively brighter spots highlighted by arrows in TEM images of Core (Figure 2c) and CS (Figure 2e) samples are putative intracrystallite mesopores. The mesopores are more evident in CS, although textural analysis reveals no observable difference in mesopore volume. It is possible that during core-shell growth a solid-state reorganization[8a] accompanies the aforementioned migration of Al from the core to the shell. TEM images of annealed samples CA (Figure 2d) and CSA (Figure 2f) clearly show an increased population of intracrystalline mesopores (indicated with ellipses). The mesopores in CA have more irregular slit-like shapes and appear to be nonuniformly distributed, whereas those in CSA are more densely populated and uniformly dispersed. This is more evident in high magnification images CA (Figure 2g) and CSA (Figure 2h). The pore size distribution analysis using density functional theory (DFT) in Figure S7 also reveals that the annealed samples have relatively larger pores (> 4 nm) than the non-annealed samples.

To assess the impact of surface passivation and intracrystalline mesoporosity on *BEA catalytic performance, we used levulinic acid (LA) esterification with *n*-butanol (*n*BuOH) as a benchmark reaction (Figure 3a). The reagent LA is a platform biomass molecule[20] used to generate *n*-butyl levulinate (*n*BuLev).[21-22, 24] Prior studies have identified *BEA as an ideal zeolite catalyst for this reaction, where it is reported that *n*BuLev is a sole product of the reaction between LA and *n*BuOH.[23a, 23d, 35] Due to ubiquitous thermodynamic limitations of esterification, this reaction is typically carried out in excess alcohol;[23d] however, it is reported that excessive alcohol concentrations in various esterification reactions can form molecular clusters on zeolite surfaces, which prevents the adsorption of carboxylic acid molecules, thus reducing the efficiency of the reaction.[36] This is also true for LA esterification to *n*BuLev where previous studies report reduced *n*BuLev production with increased *n*BuOH.[23a, 23b] To this end, we selected two different *n*BuOH-to-LA ratios for catalytic studies of core and core-shell samples.

Reactions with reduced alcohol content (*n*BuOH-to-LA = 25:1) were performed using an adapted batch protocol[11a] wherein we fix the quantity of catalyst (1.4 mol % BAS relative to LA) for each experiment. Reactions were performed at 120 °C with product yields evaluated at two different times (8 and 27 h). When the conventional *BEA catalyst (Core) is replaced with the annealed core-shell (CSA), the yield of *n*BuLev increases by a net 16% (Figure 3b) within the total timeframe of the experiment. In order to deconvolute the effects of surface passivation and enhanced mesoporosity, we compare the control (Core) to samples CS and CA, respectively. The introduction of a shell without annealing (CS) leads to surface passivation without enhancement of intracrystalline mesoporsity. Alternatively, direct annealing of the seeds (CA) leads to enhanced intracrystalline (and some interparticle) mesoporosity without detectable changes in surface composition. In Figure 3b we observe similar increases in *n*BuLev

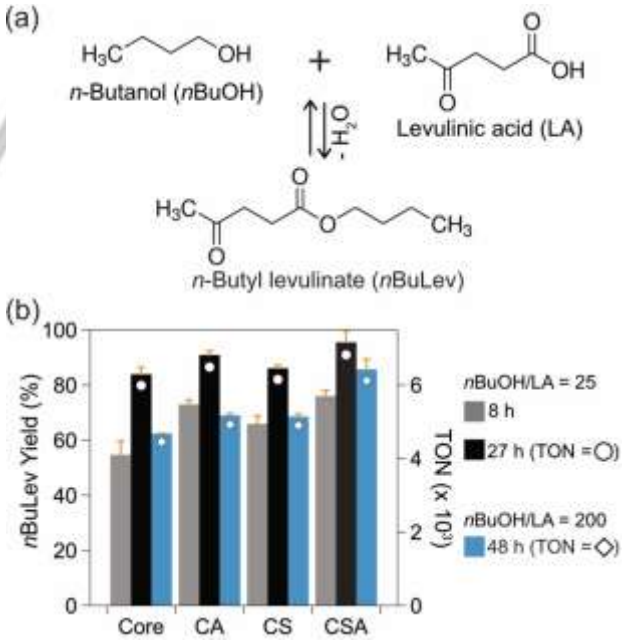


**Figure 3.** (a) Esterification of levulinic acid (LA) with *n*-butanol (*n*BuOH) to *n*-butyl levulinate (*n*BuLev) carried out at 120 °C. (b) Left axis (histograms): *n*BuLev yield (%) from reactions with Core, CA, CS, and CSA catalysts is reported relative to the initial amount of LA. The reaction using a molar ratio of *n*BuOH to LA = 25:1 is evaluated after 8 h (grey) and 27 h (black). The reaction using a molar ratio of *n*BuOH to LA = 200:1 is evaluated after 48 h (blue). Right axis (open symbols): turnover number (TON) calculated from data in Table S1 using the procedure described in the Supporting Information.



Accepted Manuscript

This article is protected by copyright. All rights reserved.

yield for both samples, suggesting that each effect positively enhances the performance of *BEA catalysts in a comparable way. The turnover number (TON) for each sample after 27 h of reaction shows an identical trend as the *n*BuLev yield (Figure 3b). Therefore, we hypothesize the net increase in CSA performance is attributed to a combination of both surface passivation and enhanced mesoporosity.

Reactions with increased alcohol content (*n*BuOH-to-LA = 200:1) lead to an expected reduction in the overall reaction rate, which required a shift to longer reaction time (48 h). As shown in Figure 3b, the general trends for TON (open symbols) and *n*BuLev yield (blue histograms) remain the same with CSA showing an even greater enhancement in product yield (i.e., a net 24% increase in *n*BuLev over that of the Core sample). It could be surmised from these collective observations that the Si-rich (hydrophobic) shells of CS and CSA diminish the formation of *n*BuOH solvent clusters on zeolite surfaces, thereby increasing molecular diffusion and the overall rate of reaction. A similar effect could be rationalized for samples CA and CSA due to the reduced silanol density that occurs during intracrystalline mesopore formation. Indeed, this reduced density of defects in mesoporous *BEA catalysts likely contributes to their reported improvement in the efficiency of LA esterification.[23b, 23c] We also confirmed an improved catalytic activity of CSA over Core using a pseudo first order reaction. Reactions at three temperatures (80, 100, 120 °C) resulted in similar activation barriers for LA esterification (62 and 60 kJ/mol for CSA and Core, respectively), and ca. 2.5-times higher pre-exponential constant for CSA (Table S2). The activation barriers found here are slightly higher than the activation barrier for esterification of ethanol and acetic acid to ethyl acetate in *BEA (ca. 50 kJ/mol).[36a] This analysis verifies a higher frequency of reactant collisions in sample CSA, consistent with its superior catalytic performance. Our findings also reveal that shell growth must involve annealing to synergistically form intracrystalline mesoporosity, introduce a more siliceous shell, and reduce the internal silanol density in *BEA structures.

## Conclusion

In this study, we have investigated the synthesis of core-shell *BEA for the purpose of introducing a more siliceous shell on the exterior rim of the zeolite. A multi-step hydrothermal growth and annealing process was evaluated using a combination of ToF-SIMS, XPS, TEM, and DLS to confirm a complex mechanism involving dissolution (i.e., desilication and dealumination) and reprecipitation to generate core-shell *BEA with a Si-rich shell (Si/Al = 53) relative to its parent core (Si/Al = 25). We also demonstrate that this process leads to the generation of hierarchical structures with intracrystalline mesoporosity, which seemingly originate from the inherent defects in *BEA particles used as seeds for core-shell synthesis. Attempts to introduce mesoporosity directly into the core (sample CA) resulted in particle breakage, which was not observed for the annealed core-shell (sample CSA). Cross-sectional TEM images of CA revealed more irregular mesopores, whereas those in CSA are relatively uniform and dispersed throughout the particle. The annealing step was found to be critical for increasing the hydrophobicity of the outer shell, as well as reducing the density of internal silanols. Catalytic testing using the LA esterification reaction revealed distinct differences among samples. Both intracrystalline mesoporosity and surface passivation were found to enhance *n*BuLev yield; however, the core-shell sample combining both features exhibited the highest performance in reactions that tested a range of *n*BuOH-to-LA ratios. These studies confirm the synergistic effects of hierarchical core-shell configurations. To our knowledge, this is the first study reporting isostructural core-shell *BEA synthesis involving the epitaxial growth of a Si-rich shell. This process also provides a more efficient route to introduce intracrystalline mesopores in zeolite beta compared to conventional post-synthesis methods. Since *BEA is widely used as a scaffold for incorporating various metals, our findings may prove to be a more generalized approach to enhance the performance of zeolite beta catalysts for other reactions. In the future, it may even be possible to perform multi-stage growth in a single-vessel to minimize synthesis steps for improved efficiency of core-shell processing.

## Acknowledgements

This work was supported by BASF Corporation. Additional support for JDR was provided by The Welch Foundation (Award E-1794). ToF-SIMS analysis was carried out with support provided by the National Science Foundation CBET-1626418. This work was conducted in part using resources of the Shared Equipment Authority at Rice University. JGM received funding for this project from the European Union's Horizon 2020 research and innovation program under grant agreement No 872102. JGM and NL thank the Spanish Ministry of Science and Innovation and AEI/FEDER, UE through the project ref. RTI2018-099504-B-C21. NL acknowledges additional support from the University of Alicante (UATALENTO17-05).

**Keywords:** zeolite • core-shell • surface passivation • mesoporosity • biomass conversion

[1] a) A. Corma, M. Moliner, Á. Cantín, M. J. Díaz-Cabañas, J. L. Jordá, D. Zhang, J. Sun, K. Jansson, S. Hovmöller, X. Zou, *Chem. Mater.* **2008**, *20*, 3218-3223; b) G. Majano, L. Delmotte, V. Valtchev, S. Mintova, *Chem. Mater.* **2009**, *21*, 4184-4191; c) D. M. Roberge, H. Hausmann, W. F. Hölderich, *Phys. Chem. Chem. Phys.* **2002**, *4*, 3128-3135.

[2] a) T. Lu, W. Yan, R. Xu, *Inorganic Chemistry Frontiers* **2019**, *6*, 1938-1951; b) M. A. Camblor, A. Corma, S. Valencia, *Chem. Commun.* **1996**, 2365-2366; c) M. M. J. Treacy, J. M. Newsam, *Nature* **1988**, *332*, 249-251.

[3] L. Bonetto, M. A. Camblor, A. Corma, J. Pérez-Pariente, *Appl. Catal. A: Gen.* **1992**, *82*, 37-50.

[4] K. Tarach, K. Góra-Marek, J. Tekla, K. Brylewska, J. Datka, K. Mlekodaj, W. Makowski, M. C. Igualada López, J. Martínez Triguero, F. Rey, *J. Catal.* **2014**, *312*, 46-57.

[5] K. S. N. Reddy, B. S. Rao, V. P. Shiralkar, *Appl. Catal. A: Gen.* **1993**, *95*, 53-63.

[6] P. Botella, A. Corma, J. M. López-Nieto, S. Valencia, R. Jacquot, *J. Catal.* **2000**, *195*, 161-168.

[7] a) J. C. Vega-Vila, J. W. Harris, R. Gounder, *J. Catal.* **2016**, *344*, 108-120; b) C.-C. Chang, S. K. Green, C. L. Williams, P. J. Dauenhauer, W. Fan, *Green Chem.* **2014**, *16*, 585-588.

[8] a) T. Ikuno, W. Chaikittisilp, Z. Liu, T. Iida, Y. Yanaba, T. Yoshikawa, S. Kohara, T. Wakihara, T. Okubo, *J. Am. Chem. Soc.* **2015**, *137*, 14533-14544; b) N. D. Hould, A. Foster, R. F. Lobo, *Microporous Mesoporous Mater.* **2011**, *142*, 104-115; c) N. D. Hould, S. Kumar, M. Tsapatsis, V. Nikolakis, R. F. Lobo, *Langmuir* **2010**, *26*, 1260-1270; d) N. D. Hould, R. F. Lobo, *Chem. Mater.* **2008**, *20*, 5807-5815.

[9] M. Trueman, D. Akporiaye, M. Anderson, *Faraday Discuss.* **2022**, *34*, 240-241.

[10] a) P. A. Wright, W. Zhou, J. Pérez-Pariente, M. Arranz, *J. Am. Chem. Soc.* **2005**, *127*, 494-495; b) J. M. Newsam, M. M. J. Treacy, W. T. Koetsier, C. B. D. Gruyter, J. M. Thomas, *Proc. R. Soc. A: Math. Phys. Eng. Sci.* **1988**, *420*, 375-405.



Accepted Manuscript

This article is protected by copyright. All rights reserved.

[11] a) L. Bui, H. Luo, W. R. Gunther, Y. Román-Leshkov, *Angew. Chem. Int. Ed.* **2013**, *52*, 8022-8025; b) D. Han, J. E, Y. Deng, J. Chen, E. Leng, G. Liao, X. Zhao, C. Feng, F. Zhang, *Renew. Sust. Energ. Rev.* **2021**, *135*, 110079-110079; c) D. T. Bregante, D. W. Flaherty, *J. Am. Chem. Soc.* **2017**, *139*, 6888-6898; d) L. Qi, M. Babucci, Y. Zhang, A. Lund, L. Liu, J. Li, Y. Chen, A. S. Hoffman, S. R. Bare, Y. Han, B. C. Gates, A. T. Bell, *J. Am. Chem. Soc.* **2021**, *143*, 21364-21378; e) L. Qi, Y. Zhang, M. A. Conrad, C. K. Russell, J. Miller, A. T. Bell, *J. Am. Chem. Soc.* **2020**, *142*, 14674-14687; f) E. Z. Ayla, D. S. Potts, D. T. Bregante, D. W. Flaherty, *ACS Catal.* **2020**, 139-154; g) D. T. Bregante, A. M. Johnson, A. Y. Patel, E. Z. Ayla, M. J. Cordon, B. C. Bukowski, J. Greeley, R. Gounder, D. W. Flaherty, *J. Am. Chem. Soc.* **2019**, *141*, 7302-7319; h) Y. Wang, J. D. Lewis, Y. Román-Leshkov, *ACS Catal.* **2016**, *6*, 2739-2744; i) C.-C. Chang, H. Je Cho, J. Yu, R. J. Gorte, J. Gulbinski, P. Dauenhauer, W. Fan, *Green Chem.* **2016**, *18*, 1368-1376; j) R. E. Patet, M. Koehle, R. F. Lobo, S. Caratzoulas, D. G. Vlachos, *J. Phys. Chem. C* **2017**, *121*, 13666-13679; k) E. Nikolla, Y. Román-Leshkov, M. Moliner, M. E. Davis, *ACS Catal.* **2011**, *1*, 408-410; l) R. Bermejo-Deval, M. Orazov, R. Gounder, S. J. Hwang, M. E. Davis, *ACS Catal.* **2014**, *4*, 2288-2297; m) R. Gounder, M. E. Davis, *ACS Catal.* **2013**, *3*, 1469-1476.

[12] T. T. Le, A. Chawla, J. D. Rimer, *J. Catal.* **2020**, *391*, 56-68.

[13] a) D. J. Yang, *Vol. US4452909A*, E. I. Du Pont de Nemours and Company, Wilmington, Del., US, **1982**; b) P. G. Rodewald, *Vol. US4402867A*, Mobil Oil Corporation, New York, N.Y., US, **1981**.

[14] a) J. Zheng, X. Zhang, Y. Wang, Y. Bai, W. Sun, R. Li, *J. Porous Mater.* **2009**, *16*, 731-736; b) J. Zheng, Q. Zeng, Y. Zhang, Y. Wang, J. Ma, X. Zhang, W. Sun, R. Li, *Chem. Mater.* **2010**, *22*, 6065-6074.

[15] a) Y. Bouizi, I. Diaz, L. Rouleau, V. P. Valtchev, *Adv. Funct. Mater.* **2005**, *15*, 1955-1960; b) J. Wang, D.-M. Do, G.-K. Chuah, S. Jaenicke, *ChemCatChem* **2013**, *5*, 247-254.

[16] a) P. J. Kunkeler, D. Moeskops, H. van Bekkum, *Microporous Mater.* **1997**, *11*, 313-323; b) S. Hu, J. Liu, G. Ye, X. Zhou, M.-O. Coppens, W. Yuan, *Angew. Chem. Int. Ed.* **2021**, anie.202104859-anie.202104859; c) N. N. M. Ghani, A. A. Jalil, S. Triwahyono, M. A. A. Aziz, A. F. A. Rahman, M. Y. S. Hamid, S. M. Izan, M. G. M. Nawawi, *Chem. Eng. Sci.* **2019**, *193*, 217-229; d) P. Andy, J. Garcia-Martinez, G. Lee, H. Gonzalez, C. W. Jones, M. E. Davis, *J. Catal.* **2000**, *192*, 215-223.

[17] B. Xie, H. Zhang, C. Yang, S. Liu, L. Ren, L. Zhang, X. Meng, B. Yilmaz, U. Müller, F.-S. Xiao, *Chem. Commun.* **2011**, *47*, 3945-3945.

[18] a) A. Ghorbanpour, A. Gumidyala, L. C. Grabow, S. P. Crossley, J. D. Rimer, *ACS Nano* **2015**, *9*, 4006-4016; b) T. T. Le, K. Shilpa, C. Lee, S. Han, C. Weiland, S. R. Bare, P. J. Dauenhauer, J. D. Rimer, *J. Catal.* **2022**, *405*, 664-675.

[19] a) A. G. Machoke, A. M. Beltrán, A. Inayat, B. Winter, T. Weissenberger, N. Kruse, R. Güttel, E. Spiecker, W. Schwieger, *Adv. Mater.* **2015**, *27*, 1066-1070; b) W. Schwieger, A. G. Machoke, T. Weissenberger, A. Inayat, T. Selvam, M. Klumpp, A. Inayat, *Chem. Soc. Rev.* **2016**, *45*, 3353-3376; c) M. Jin, M. Oh, M. Choi, *ACS Catal.* **2022**, *12*, 4067-4077; d) S. W. Han, H. Park, J. Han, J.-c. Kim, J. Lee, C. Jo, R. Ryoo, *ACS Catal.* **2021**, 9233-9241; e) R. Ryoo, J. Kim, C. Jo, S. W. Han, J. C. Kim, H. Park, J. Han, H. S. Shin, J. W. Shin, *Nature* **2020**, *585*, 221-224; f) H. Chen, J. Wydra, X. Zhang, P.-S. Lee, Z. Wang, W. Fan, M. Tsapatsis, *J. Am. Chem. Soc.* **2011**, *133*, 12390-12393.

[20] a) J. C. Serrano-Ruiz, J. A. Dumesic, *Energy & Environmental Science* **2011**, *4*, 83-99; b) J. J. Bozell, G. R. Petersen, *Green Chem.* **2010**, *12*, 539-554; c) W. P. Xu, X. F. Chen, H. J. Guo, H. L. Li, H. R. Zhang, L. Xiong, X. D. Chen, *J. Chem. Technol. Biotechnol.* **2021**, *96*, 3009-3024.

[21] a) M. S. Tiwari, J. S. Dicks, J. Keogh, V. V. Ranade, H. G. Manyar, *Mol. Catal.* **2020**, *488*, 110918; b) S. A. Ariffin Kashinath, Z. Abdul Manan, H. Hashim, S. R. Wan Alwi, *Comput. Chem. Eng.* **2012**, *41*, 88-92.

[22] a) A. D. Moreno, P. Alvira, D. Ibarra, E. Tomás-Pejó, in *Production of Platform Chemicals from Sustainable Resources* (Eds.: Z. Fang, J. R. L. Smith, X. Qi), Springer Singapore, Singapore, **2017**, pp. 375-410; b) C. Leibig, B. Mullen, T. Mullen, L. Rieth, V. Badarinarayana, in *Renewable and Sustainable Polymers, Vol. 1063*, American Chemical Society, **2011**, pp. 111-116.

[23] a) K. C. Maheria, J. Kozinski, A. Dalai, *Catal. Lett.* **2013**, *143*, 1220-1225; b) D. H. Morawala, A. K. Dalai, K. C. Maheria, *Catal. Lett.* **2020**, *150*, 1049-1060; c) D. H. Morawala, D. R. Lathiya, A. K. Dalai, K. C. Maheria, *Catal. Today* **2020**, *348*, 177-186; d) J. Yang, G. Li, L. Zhang, S. Zhang, *Catalysts* **2018**, *8*, 14-14.

[24] a) Z. Babaei, A. Najafi Chermahini, M. Dinari, *Colloids Surf. Physicochem. Eng. Aspects* **2021**, *625*, 126885-126885; b) G. Shrivastav, T. S. Khan, M. Agarwal, M. A. Haider, *ACS Sustain. Chem. Eng.* **2017**, *5*, 7118-7127.

[25] L. Ding, Y. Zheng, *Mater. Res. Bull.* **2007**, *42*, 584-590.

[26] J. J. De Yoreo, P. U. P. A. Gilbert, N. A. J. M. Sommerdijk, R. L. Penn, S. Whitelam, D. Joester, H. Zhang, J. D. Rimer, A. Navrotsky, J. F. Banfield, A. F. Wallace, F. M. Michel, F. C. Meldrum, H. Colfen, P. M. Dove, *Science* **2015**, *349*, 6760-6760.

[27] a) H. Dai, C. Lee, W. Liu, T. Yang, J. Claret, X. Zou, P. J. Dauenhauer, X. Li, J. D. Rimer, *Angew. Chem. Int. Ed. Engl.* **2022**, *61*, e202113077; b) H. Dai, Y. Shen, T. Yang, C. Lee, D. Fu, A. Agarwal, T. T. Le, M. Tsapatsis, J. C. Palmer, B. M. Weckhuysen, P. J. Dauenhauer, X. Zou, J. D. Rimer, *Nat. Mater.* **2020**, *19*, 1074-1080.

[28] J. Pérez-Ramírez, S. Abelló, A. Bonilla, J. C. Groen, *Adv. Funct. Mater.* **2009**, *19*, 164-172.

[29] L. Karwacki, M. H. F. Kox, D. A. Matthijs de Winter, M. R. Drury, J. D. Meeldijk, E. Stavitski, W. Schmidt, M. Mertens, P. Cubillas, N. John, A. Chan, N. Kahn, S. R. Bare, M. Anderson, J. Kornatowski, B. M. Weckhuysen, *Nat. Mater.* **2009**, *8*, 959-965.

[30] a) X. Zhou, M. Wang, D. Yan, Q. Li, H. Chen, *J. Catal.* **2019**, *379*, 138-146; b) N. V. Vlasenko, Y. N. Kochkin, G. M. Telbiz, O. V. Shvets, P. E. Strizhak, *RSC Adv.* **2019**, *9*, 35957-35968.

[31] a) H. Sammoury, J. Toufaily, K. Cherry, T. Hamieh, Y. Pouilloux, L. Pinard, *Microporous Mesoporous Mater.* **2018**, *267*, 150-163; b) J. García-Martínez, M. Johnson, J. Valla, K. Li, J. Y. Ying, *Catal. Sci. Technol.* **2012**, *2*, 987-987; c) J. C. Groen, G. M. Hamminga, J. A. Moulijn, J. Pérez-Ramírez, *Phys. Chem. Chem. Phys.* **2007**, *9*, 4822-4830; d) J. C. Groen, J. C. Jansen, J. A. Moulijn, J. Pérez-Ramírez, *J. Phys. Chem. B* **2004**, *108*, 13062-13065; e) J. C. Groen, L. A. A. Peffer, J. A. Moulijn, J. Pérez-Ramírez, *Microporous Mesoporous Mater.* **2004**, *69*, 29-34; f) I. C. Medeiros-Costa, E. Dib, N. Nesterenko, J.-P. Dath, J.-P. Gilson, S. Mintova, *Chem. Soc. Rev.* **2021**, *50*, 11156-11179; g) J. C. Groen, S. Abelló, L. A. Villaescusa, J. Pérez-Ramírez, *Microporous Mesoporous Mater.* **2008**, *114*, 93-102; h) A. Sachse, A. Grau-Atienza, E. O. Jardim, N. Linares, M. Thommes, J. García-Martínez, *Cryst. Growth Des.* **2017**, *17*, 4289-4305.

[32] a) D. Verboekend, J. Pérez-Ramírez, *Catalysis Science and Technology* **2011**, *1*, 879-890; b) K. Sadowska, K. Góra-Marek, M. Drozdek, P. Kuśtrowski, J. Datka, J. Martinez Triguero, F. Rey, *Microporous Mesoporous Mater.* **2013**, *168*, 195-205.

[33] D. T. Bregante, M. C. Chan, J. Z. Tan, E. Z. Ayla, C. P. Nicholas, D. Shukla, D. W. Flaherty, *Nat. Catal.* **2021**, *4*, 797-808.

[34] K. Lee, S. Lee, Y. Jun, M. Choi, *J. Catal.* **2017**, *347*, 222-230.

[35] S. Dharne, V. V. Bokade, *Journal of Natural Gas Chemistry* **2011**, *20*, 18-24.

[36] a) J. Bedard, H. Chiang, A. Bhan, *J. Catal.* **2012**, *290*, 210-219; b) S. R. Kirumakki, N. Nagaraju, S. Narayanan, *Appl. Catal. A: Gen.* **2004**, *273*, 1-9.

Accepted Manuscript



This article is protected by copyright. All rights reserved.

10.1002/anie.202210434



## Entry for the Table of Contents

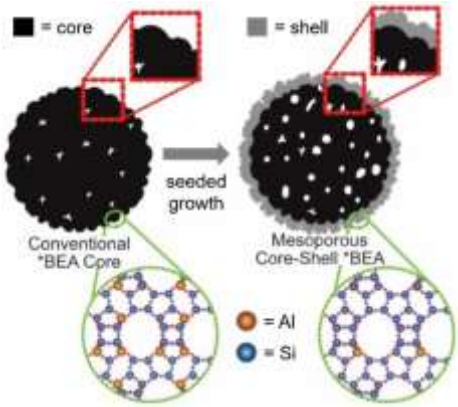


The synthesis of core-shell zeolite beta (*BEA) produces a zeolite with an epitaxially grown Si-rich shell on the exterior rim, which passivates the surface reactivity. It is also possible to enhance intracrystalline mesoporosity via secondary hydrothermal treatment by taking advantage of intrinsic silanol defects in *BEA.

WILEY-VCH
Accepted Manuscript


This article is protected by copyright. All rights reserved.